Non-intrusive Impedance Characterization of Two-Port Electrical Devices by Inductive Probes

Simone Negri, *Senior Member*, *IEEE,* Giordano Spadacini, *Senior Member, IEEE*, Flavia Grassi, *Senior Member, IEEE*, and Sergio A. Pignari, *Fellow, IEEE*

***Abstract*— Many industry applications related to power electronics, including electromagnetic interference (EMI) filtering, control system stability analysis, and electrical equipment monitoring, require broadband impedance measurements. To this aim, inductive probes have been proposed as non-intrusive signal couplers clamped on wiring harness, to carry out in-circuit impedance measurements while the system under test is normally operating. Previous contributions on this subject include either one-port methods, unsuitable for multiport systems, or multiport methods developed for admittance-matrix measurement. Besides, those methods were assessed up to 30 MHz while the current CISPR-25 automotive standard extends conducted-EMI verifications up to 110 MHz. In this paper, an inductively-coupled measurement procedure is formulated for two-port impedance-matrix characterization. After discussing probe selection criteria, the proposed test setup is validated by ad-hoc passive networks, whose impedance matrix can be independently and accurately evaluated. Comparison with the obtained measurement data proves good accuracy from 150 kHz to 110 MHz. Results obtained by using different pairs of probes and the role played by the number of cable turns are also discussed. As a real automotive application example, a lead-acid battery is characterized in terms of physical and modal impedance parameters.**

***Index Terms*— In-circuit impedance measurement, in-circuit admittance measurement, behavioral models, EMI, EMC.**

I. INTRODUCTION

THE experimental characterization of electrical devices in terms of frequency responses is of great interest in industry applications. Given the inherent variability of the frequency response with functional operating conditions (e.g. different voltage and power levels), the measurement process should be carried out on operating equipment, which is easily achieved by in-circuit impedance measurements. This family of characterization techniques is of particular interest for electromagnetic interference (EMI) modelling, including design of common-mode (CM) [1] and EMI [2] filters, performance analysis of single-phase [3], [4] and three-phase [5], [6] filters for EMI mitigation, and broadband behavioral modelling of electronic power converters [7], [8]. In addition to EMI, in-circuit (or online) impedance measurements find application in microgrid stability analysis [9] and electrical equipment monitoring, such as asynchronous motor turn-fault [10] and inter-fault [11] diagnosis. Batteries represent and additional use-case of interest, as their impedance is often used for parameter estimation purposes [12] or state of health assessing for second-life applications [13]. More interestingly, battery impedance can be measured online to monitor its internal parameters [14], temperature [15], or to recognize faults [16]. Additionally, EMI analysis and functional monitoring techniques can be combined, as variations in EMI can be related to specific fault conditions [17].

In this context, inductively coupled measurement techniques, performed by clamping inductive probes on the cable harness of the equipment under test (EUT) are of particular interest owing to their practicality (i.e., performing in-circuit measurement while the system under test is operating) and safety [18]. Two families of inductively coupled impedance measurement techniques are known: two-probe setup (TPS) [19] and single-probe setup (SPS) [20]. The TPS [21] was originally developed as a non-intrusive measurement technique for power lines monitoring and diagnosis purposes, and it was later refined and applied to a broad range of applications, including transformers [22], PV systems [23], and general electrical equipment [24] monitoring. Additionally, the TPS was successfully used as a tool in EMI analysis [2], with recent contributions addressing how to tune the setup sensitivity by additional external windings on each probe [25] and methods to reduce noise effects for the characterization of active EUTs [26]. Regardless of its strengths, the coupling effect between probes is a well-known issue of the TPS, which requires specific mitigation techniques [27]. In order to avoid the probe coupling issue, the SPS was proposed, which also benefits from a reduction in setup complexity [5], [28]. The SPS was

This study was carried out within the MOST – Sustainable Mobility Center and received funding from the European Union Next-Generation EU (PIANO NAZIONALE DI RIPRESA E RESILIENZA (PNRR) - MISSIONE 4 COMPONENTE 2, INVESTIMENTO 1.4 - D.D. 1033 17/06/2022, CN00000023). This manuscript reflects only the authors' views and opinions, neither the European Union nor the European Commission can be considered responsible for them.

The authors are with the Department of Electronics, Information and Bioengineering, Politecnico di Milano, 20133 Milan, Italy (e-mail: simone.negri@polimi.it; giordano.spadacini@polimi.it; flavia.grassi@polimi.it; sergio.pignari@polimi.it).

Color versions of one or more of the figures in this article are available online at http://ieeexplore.ieee.org

Published version available, doi: 10.1109/TIA.2025.3606425.

successfully applied to the characterization of physical [5] and modal - differential mode (DM) [29] and CM [30] - single impedances of common electrical drives, and eventually extended to time-domain measurements of time-varying impedances [31]. The sensitivity of the SPS can also be improved by suitably winding the EUT cable the probe is clamped on [5].

However, both SPS and TPS measurement methods are suitable for single (one-port) impedances only, and are unsuitable for the measurement of the full impedance matrices needed to properly characterize multiport systems.

The problem of the non-intrusive characterization of multiport systems was addressed by an inductively coupled multi-port and multi-probe measurement setup (MPS) [32], which allowed the identification of physical [32] and modal [33] admittance matrices. The admittance parameters (unlike the impedance ones) allow the straightforward identification of a behavioral circuit model of the EUT [3], [34] in form of a Norton equivalent circuit.

However, an industrial solution for the non-intrusive identification of impedance matrices, often needed to determine a behavioral model of the EUT in form of a Thevenin equivalent circuit, is currently lacking. While, in principle, an impedance matrix can be obtained by inversion of the admittance one, this introduces an additional mathematical operation which can severely affect the accuracy of results.

In this context, this paper presents an alternative formulation of the in-circuit admittance measurement technique [32], originally introduced in [35], where the one-port SPS was extended to a two-port formulation, resulting in an inductively coupled, in-circuit measurement technique suitable to directly determine full impedance matrices. Specifically, the results presented in [35], originally limited to a frequency range spanning from 150 kHz to 30 MHz and hence insufficient for application in automotive setups [36], are here extended to a broader frequency range, reaching up to 110 MHz, so to cover the full CISPR-25 frequency range. This is possible thanks to the selection of specific inductive probes, based on in-depth theoretical analysis of the probe-to-circuit coupling mechanism and its dependence on probe turns ratio. Extensive experimental results are presented to support the proposed methods, highlighting their advantages and limitations. First, a comparison among three different measurement setups relying on different probes is presented to validate the considered probe selection criteria. Second, to highlight the method accuracy under controlled conditions, the proposed method is validated with a set of known test networks. Lastly, to demonstrate how the proposed method can be practically implemented on a real-world system, the characterization procedure of a lead-acid battery is presented, including a method for the de-embedding of setup cables and LISNs.

The paper is structured as follows: The considered measurement setup, the measurement problem formulation, and the calibration method are detailed in Section II. Criteria for optimal probe selection are discussed in Section III. The proposed measurement technique is then applied, in the frequency range from 150 kHz to 110 MHz, to the characterization of a passive test network in Section IV, and the results obtained by different probes are compared. An application example is discussed in Section V, including a method for de-embedding cables and LISNs. Eventually, final conclusions and remarks are reported in Section VI.

II. Matrix In-Circuit Impedance Measurement

A. Measurement Principle

Consider a measurement setup consisting of a vector network analyzer (VNA), an EUT with two electrical ports, and a couple of inductive probes, generally different from each other, as shown in Fig. 1. This paper is aimed at the development of a procedure for the identification of the unknown 2×2 impedance matrix $\mathbf{Z}_x$, representing the considered EUT only, on the basis of the 2×2 S-parameters matrix $\mathbf{S}_m$, which represents the whole setup and is directly obtained from the VNA measurements. The latter matrix is used to express reflected power waves b_1, b_2 as a linear combination of incident power waves a_1, a_2, according to:

$$\begin{bmatrix} b_1 \\ b_2 \end{bmatrix} = \underbrace{\begin{bmatrix} S_{m11} & S_{m12} \\ S_{m21} & S_{m22} \end{bmatrix}}_{\mathbf{S}_m} \begin{bmatrix} a_1 \\ a_2 \end{bmatrix}, \tag{1}$$

and can be readily converted to the corresponding measured impedance matrix $\mathbf{Z}_m$, namely:

$$\mathbf{Z}_m = Z_0 \left(\mathbf{I}_2 + \mathbf{S}_m\right)\left(\mathbf{I}_2 - \mathbf{S}_m\right)^{-1}, \tag{2}$$

where the 2×2 identity matrix is denoted as $\mathbf{I}_2$, and the standard S-parameter reference impedance is denoted as Z_0, with $Z_0 = 50$ Ω. With reference to Fig. 1 for the notation of port voltages and currents, the following relationships hold:

$$\begin{bmatrix} v_1 \\ v_2 \end{bmatrix} = \underbrace{\begin{bmatrix} Z_{m11} & Z_{m12} \\ Z_{m21} & Z_{m22} \end{bmatrix}}_{\mathbf{Z}_m} \begin{bmatrix} i_1 \\ i_2 \end{bmatrix}, \tag{3}$$

$$\begin{bmatrix} v_1 \\ i_1 \end{bmatrix} = \underbrace{\begin{bmatrix} A_1 & B_1 \\ C_1 & D_1 \end{bmatrix}}_{\mathbf{T}_1} \begin{bmatrix} v_{x1} \\ i_{x1} \end{bmatrix}, \begin{bmatrix} v_2 \\ i_2 \end{bmatrix} = \underbrace{\begin{bmatrix} A_2 & B_2 \\ C_2 & D_2 \end{bmatrix}}_{\mathbf{T}_2} \begin{bmatrix} v_{x2} \\ i_{x2} \end{bmatrix}, \tag{4}$$

where $\mathbf{T}_1$, $\mathbf{T}_2$ are the transmission (ABCD) matrices representing, respectively, probes 1 and 2. As detailed in [35], it is possible to express voltages v_{x1}, v_{x2}, as a function of currents i_{x1}, i_{x2}, in the form

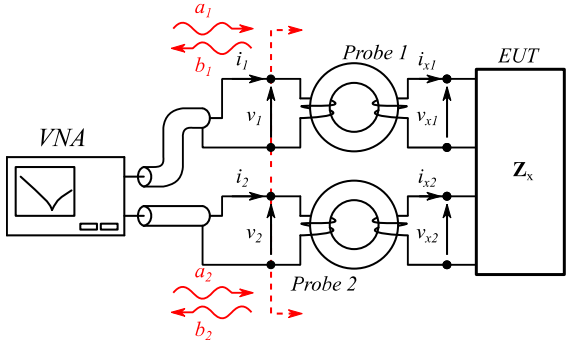

Fig. 1. Two-port impedance measurement setup under consideration.

$$\begin{bmatrix} v_{x1} \\ v_{x2} \end{bmatrix} = \underbrace{\begin{bmatrix} Z_{x11} & Z_{x12} \\ Z_{x21} & Z_{x22} \end{bmatrix}}_{\mathbf{Z}_x} \begin{bmatrix} i_{x1} \\ i_{x2} \end{bmatrix}, \tag{5}$$

where the entries of the impedance matrix $\mathbf{Z}_x$ are functions of the entries of the measured S-parameters matrix $\mathbf{S}_\mathrm{m}$ and of the entries of matrices $\mathbf{T}_1$, $\mathbf{T}_2$, defined as:

$$Z_{x11} = \frac{h_1 + h_2 S_{m11} + h_2 h_7 \det[\mathbf{S}_m] + h_1 h_7 S_{m22}}{1 + h_6 S_{m11} + h_6 h_7 \det[\mathbf{S}_m] + h_7 S_{m22}}, \tag{6}$$

$$Z_{x12} = \frac{h_3 S_{m12}}{1 + h_6 S_{m11} + h_6 h_7 \det[\mathbf{S}_m] + h_7 S_{m22}}, \tag{7}$$

$$Z_{x21} = \frac{h_3 S_{m21}}{1 + h_6 S_{m11} + h_6 h_7 \det[\mathbf{S}_m] + h_7 S_{m22}}, \tag{8}$$

$$Z_{x22} = \frac{h_4 + h_4 h_6 S_{m11} + h_5 h_6 \det[\mathbf{S}_m] + h_5 S_{m22}}{1 + h_6 S_{m11} + h_6 h_7 \det[\mathbf{S}_m] + h_7 S_{m22}}. \tag{9}$$

The seven coefficients h_1, h_2, h_3, h_4, h_5, h_5, h_6, h_7, appearing in (6)-(9), are defined as:

$$\begin{aligned} h_1 &= \frac{-B_1 + D_1 Z_0}{A_1 - C_1 Z_0},\ h_2 = \frac{B_1 + D_1 Z_0}{A_1 - C_1 Z_0}, \\ h_3 &= \frac{2 Z_0}{\left(A_1 - C_1 Z_0\right)\left(A_2 - C_2 Z_0\right)}, \\ h_4 &= \frac{-B_2 + D_2 Z_0}{A_2 - C_2 Z_0},\ h_5 = \frac{B_2 + D_2 Z_0}{A_2 - C_2 Z_0}, \\ h_6 &= \frac{A_1 + C_1 Z_0}{-A_1 + C_1 Z_0},\ h_7 = \frac{A_2 + C_2 Z_0}{-A_2 + C_2 Z_0}. \end{aligned} \tag{10}$$

It is worth noting that the equations of impedance parameters (6)-(9) are formally equivalent to the ones presented in [32] for admittance parameters, but the seven coefficients h_i (10) are different from the seven coefficient k_i used in [32].

The entries of the two probes transmission (ABCD) matrices $\mathbf{T}_1$, $\mathbf{T}_2$ are commonly not included in the data provided by manufactures. Additionally, while it is in principle possible to characterize each probe in terms of ABCD parameters, this is not usually feasible in industrial environments, as the procedure would require an ad-hoc, non-standard measurement setup. Consequently, it is easier and less time consuming to determine a calibration procedure to directly obtain the seven coefficients (10) by a set of simple experiments, so that they can then be directly used in (6)-(9), not dissimilarly from the SPS [5], [20] and MPS [32] calibration procedure.

B. Calibration Procedure

Following the same approach presented in [32], it is at first worth considering that equations (6)-(9) are, generally, fully coupled. Yet, in the case of the two EUT ports being not coupled (i.e. if a two-port network is realized by separate one-port impedances), (6)-(9) are reduced to single, separate equations. In this case, it holds S_{m12}=S_{m21}= 0, thus Z_{x12}=Z_{x21}=0 in (7), (8). By basic algebraic calculus, self-impedances expressions (6), (9) are simplified, resulting in:

$$Z_{x11}\big|_{S_{m12}=S_{m21}=0} = \frac{h_1 + h_2 S_{m11}}{1 + h_6 S_{m11}}, \tag{11}$$

$$Z_{x22}\big|_{S_{m12}=S_{m21}=0} = \frac{h_4 + h_5 S_{m22}}{1 + h_7 S_{m22}}. \tag{12}$$

It is worth considering that equations (11), (12) can be recognized as equivalent to the SPS [5], [20], separately, for each port. Consequently, as proposed in [32] for two-port admittance parameters, one can rely on the SPS calibration procedure [5], carried out, separately, for each port. The recalled calibration method relies on three reference loads with known impedances Z_A, Z_B, Z_C. By connecting to probe 1, in turn, the three reference loads, the reflection S-parameters S_{1A}, S_{1B}, S_{1C} are measured, respectively. Then, by substituting the measured reflection S-parameters and the corresponding known reference load impedances in (11), a linear system in the unknowns h_1, h_2, h_6 is obtained as

$$\begin{cases} Z_A\left(1 + h_6 S_{1A}\right) = h_1 + h_2 S_{1A} \\ Z_B\left(1 + h_6 S_{1B}\right) = h_1 + h_2 S_{1B} \\ Z_C\left(1 + h_6 S_{1C}\right) = h_1 + h_2 S_{1C} \end{cases}, \tag{13}$$

which can be solved resulting in one unique solution for the coefficients h_1, h_2, h_6. Similarly, by connecting to probe 2, in turn, the reference impedances Z_A, Z_B, Z_C, their reflection S-parameters S_{2A}, S_{2B}, S_{2C} are measured, respectively. By substituting the measured reflection S-parameters and the corresponding known reference load impedances in (12), a linear system in the unknowns h_4, h_5, h_7 is obtained, which provides, as its unique solution, the expressions of coefficients h_4, h_5, h_7.

The last coefficient h_3 is determined by a single two probe test, connecting to the probes a single reference two-port network with known impedance matrix $\mathbf{Z}_D$ and measuring the corresponding S-parameter matrix $\mathbf{S}_D$. By substituting the entries of the measured S-parameters matrix $\mathbf{S}_D$ and of the known reference load impedance matrix $\mathbf{Z}_D$ in the expressions of the mutual impedances (7), (8), h_3 is determined. Explicit solutions for the determination of the seven coefficients h_1, h_2, h_3, h_4, h_5, h_5, h_6, h_7 can be found [35].

III. Criteria for Optimal Probe Selection

For the implementation of the proposed method, one can purposely choose a pair of clamp-on inductive probes among those largely available in EMC laboratories, which are used either for current monitoring or bulk-current injection (BCI) testing. This section addresses the optimal selection criteria.

Data sheets declare a maximum operating frequency f_max which is limited by the performance of the ferrite core (that is, the amplitude response of magnetic permeability steeply falls above f_max) and by parasitic capacitive effects. Both these two detrimental effects are critical for repeatability and accuracy in the proposed application. Therefore, f_max must be greater than the highest frequency of interest for impedance measurement (in this work, 110 MHz).

Another parameter provided by probe manufacturers is the plot of an amplitude response, which represents either the transfer impedance (TI) for current-monitor probes, or the insertion loss (IL) for BCI probes. Although these figures of

merit are specific of different applications, they are of interest in the proposed method as a mean to infer the number of turns N_p of the inner winding (the primary winding) which is seldom reported in data sheets and cannot even be inspected without disassembling the probe itself, which is often a destructive operation. To this aim, one can read the maximum value of the TI and IL on the high-frequency plateau of the curve, and compare it with the theoretically maximum value produced by an ideal probe behaving as a perfect N_p:1 transformer.

Specifically, for current-monitor probes one can refer to the circuit model in Fig. 2(a) where the current I_m flowing on the clamped wire is transformed into a current I_m/N_p flowing in the probe winding, giving rise to a measured voltage V_m across the standard resistance R_0 = 50 Ω of a spectrum analyzer. Consequently, the maximum TI can be expressed in logarithmic units as

$$TI_{max} = 20\log_{10}\left(\frac{V_m}{I_m}\right) = 20\log_{10}\left(\frac{50}{N_p}\right) \tag{14}$$

Similarly, the circuit model in Fig. 2(b) represents an ideal BCI probe clamped on the calibration jig having two terminal loads R_0 (with the injected voltage V_{jig}), while the probe is fed by a radio-frequency generator (voltage source V_S in series with R_0) [37]. According to the definition of IL expressed in dB, the solution of this circuit model yields

$$IL_{max} = 20\log_{10}\left(\frac{V_{jig}}{V_S/2}\right) = 20\log_{10}\left(\frac{2N_p}{2N_p^2+1}\right) \tag{15}$$

Table I reports three probe models available in the authors' laboratory, along with their f_{max}, the actual TI_{max} or IL_{max} reported in data sheets, and the N_p inferred by the closest value computed by (14) or (15).

The application of inductive probes as couplers of VNA ports benefits from winding the clamped cable with a number of secondary turns $N_s \geq 1$. Specifically, it is shown in [5], [25], that $N_s \geq N_p$ increases measurement sensitivity (lowest and larger detectable impedance). However, two practical limitations must be considered, namely, 1) the possible cumbersomeness of the setup with large N_s and 2) the geometrical randomness of hand-made cable turns, leading to uncontrolled parasitic effects

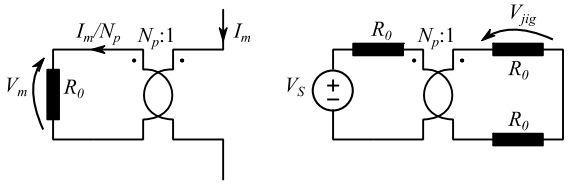

Fig. 2. Equivalent circuits with (a) monitor probe and (b) BCI probe modelled as ideal transformers.

TABLE I
AVAILABLE PROBES AND THEIR PARAMETERS

MODEL	f_{max} [MHz]	TI_{max} [dBΩ]	IL_{max} [dB]	N_p
FCC F-120-2	230	---	−7.5	2
Solar 9123-1N	400	18.4	---	6
TekBox TBBCI1-800K420	500	---	−4.4	1

which may be detrimental for high-frequency reproducibility. Therefore, the suggested trade-off criterium (without loss of generality though) is the choice $N_s = N_p$ which also leads to an equivalent 1:1 configuration regardless of the specific probe used, ideally making different probes comparable. In the experiments reported in the next sections, this criterium will be adopted for each probe in Table I unless differently specified. For instance, the general representation in Fig. 1 suggested this solution for N_s=N_p=2. In this respect, probes with N_p=1 are much more practical than the other ones, as they can be simply clamped on the cable with no need for additional turns.

IV. EXPERIMENTAL VERIFICATION

A. Experimental Setups

To exemplify and validate the proposed method, the three probe models reported in Table I were considered, with different choices of the secondary winding (i.e., the number of turns of the clamped cable). Specifically, three setups were implemented by using:

I. FCC F-120-2 and Solar 9123-1N, with a simple cable turn (i.e., N_s=1≠ N_p, unlike the solution proposed in Section III).
II. FCC F-120-2 with a two-turn cable winding, and Solar 9123-1N with a six-turn cable winding (i.e., N_s=N_p as proposed in Section III).
III. two TekBox TBBCI1-800K420, with a simple cable turn (i.e., N_s=1=N_p as proposed in Section III).

For each probe pair, a Keysight E5061B VNA was used, and the experimental setup depicted in Fig. 1 was built. Instrument settings were: Frequency from 150 kHz to 110 MHz, 100 Hz resolution bandwidth, 8 dBm forward power.

B. Setup Calibration

In this section, the calibration procedure for setup III is documented (other setups are treated analogously). Firstly, the calibration procedure requires three one-port measurements for each probe. The required setup is depicted in Fig. 3(a) for port 1, while port 2 is treated analogously. Probes secondary windings are then connected to a reference load Z_D, as shown in Fig. 3(b), and the impedance matrix needed for the two-port calibration is measured, providing the entries $Z_{D11} = Z_{D12} = Z_{D21} = Z_{D22} = Z_D$. Note that consistency among successive measurements is granted by the marked terminal on each probe

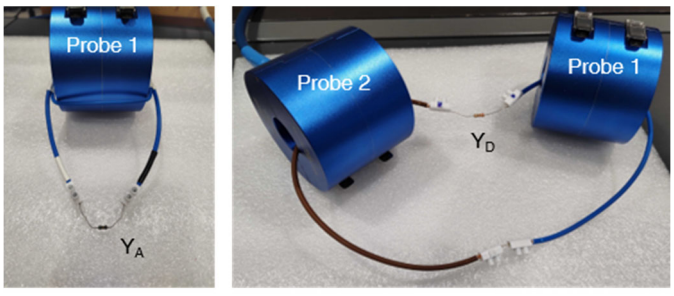

Fig. 3. Port 1 calibration setup for the determination of coefficients h_1, h_2, h_6 (a), and two-port calibration setup (b) for the determination of coefficient h_3.

winding, which highlights probes mutual orientation.

The reference loads are selected considering that their impedances must ensure that the linear systems (13) have one, unique solution. Existence and unicity of the solution are easily obtained if: (a) the test loads impedances have very different magnitudes, spanning the whole magnitude range of interest, and (b) the test load impedance magnitudes are consistently different in the frequency range of interest. Both requirements are satisfied by selecting as test loads four resistors with nominal values 1.1 Ω (A), 50 Ω (B), 1 kΩ (C), 220 Ω (D), whose impedances Z_A, Z_B, Z_C, Z_D are previously obtained by means of independent reflectometric measurements. The seven coefficients h_1, h_2, h_3, h_4, h_5, h_6, h_7 can hence be determined, and their values are reported in Fig. 4, in magnitude and phase.

C. Verification of the Proposed Method

In this section, the proposed method is verified with the setup with two probes TekBox TBBCI1-800K420. The comparison between setups with different probes is reported in the subsequent subsection.

To this end a test network is used, whose circuit is reported in Fig. 5, along with a principle representation of the whole validation setup. A picture of the corresponding real setup is reported in Fig. 6. The test network includes two resistors (R_1 = 0 Ω, R_2 = 125 Ω) and has three electrical ports: two are used as measurement ports, while the third port is terminated on a resistor (50 Ω), an inductor (10 μH), or a capacitor (47 nF),

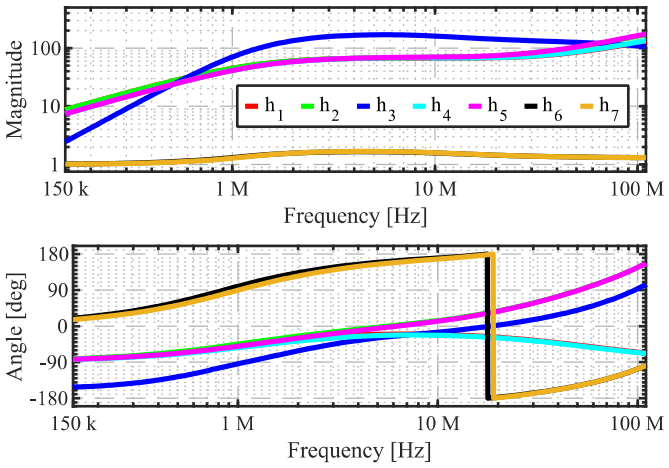

Fig. 4. Magnitude and angle of the coefficients h_1 [Ω], h_2 [Ω], h_3 [Ω], h_4 [Ω], h_5 [Ω], h_6 [unitless], h_7 [unitless].

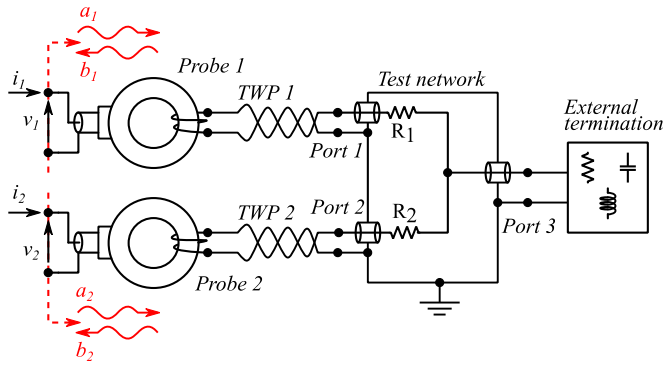

Fig. 5. Schematic of the validation setup, including: inductive probes, TWPs and test network with resistive, inductive or capacitive termination.

effectively realizing different two port networks.

To enable direct connection of a VNA to measure reference S-parameters and to have a well-controlled setup, a metallic box with external SMA connectors encloses each test network. The reference impedance parameters for validation can be mathematically obtained from the measured S-parameters.

The connection between test networks and probes is obtained by means of two short pieces of twisted-wire pairs (TWP). Their contribution must be embedded in the reference impedance values, which is easily achieved by separately characterizing each twisted wire pair in terms of per-length inductance and capacitance.

The comparison between the impedance matrix entries measured by the proposed inductively coupled technique and their reference values obtained by direct VNA connection is reported, in magnitude and angle, in Fig. 7, Fig. 8 and Fig. 9, respectively, for the test network with resistive, capacitive, and inductive termination. Note that, as the test network is reciprocal (i.e., Z_{12} = Z_{21}) only one mutual impedance is reported. It can be appreciated that the proposed measurement technique provides very good results from 150 kHz up to 110 MHz, with excellent accuracy from 150 kHz to 80 MHz and

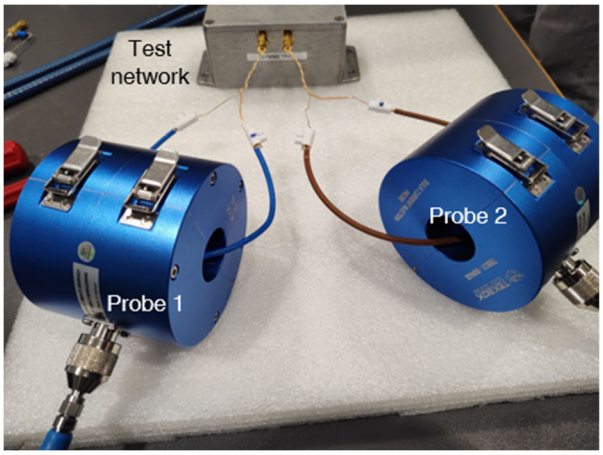

Fig. 6. Validation setup with test network (VNA not shown).

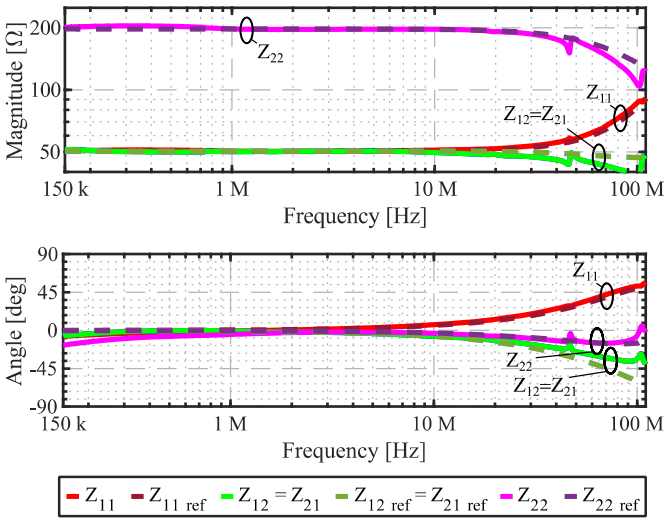

Fig. 7. Test network with resistive termination: comparison between measured (solid) and reference (dashed) values of the impedance matrix entries, in magnitude and angle.

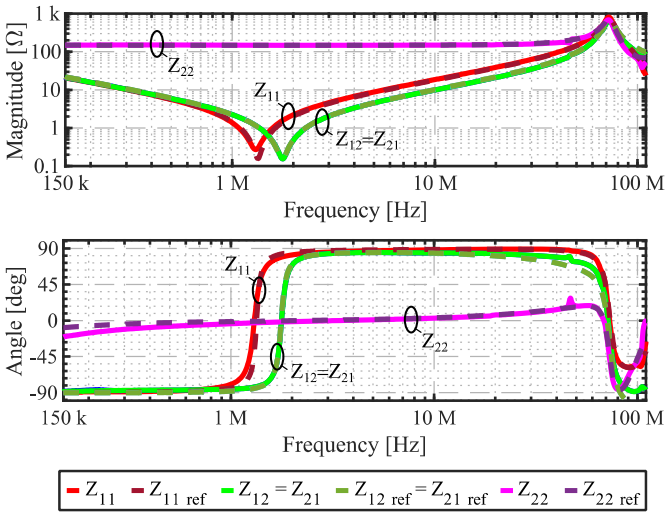

Fig. 8. Test network with capacitive termination: comparison between measured (solid) and reference (dashed) values of the impedance matrix entries, in magnitude and angle.

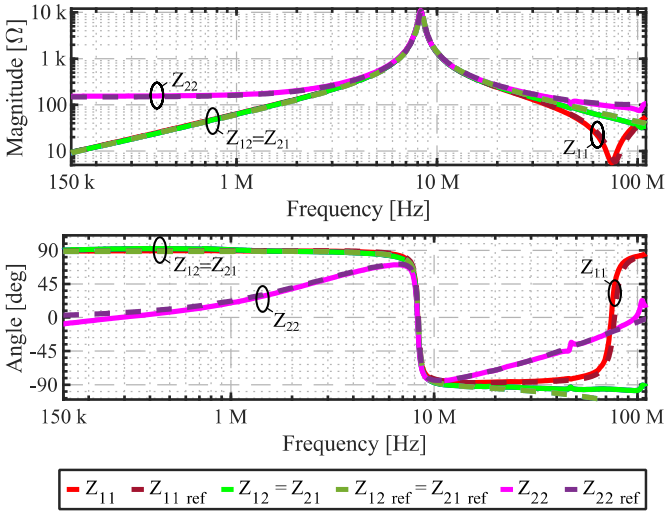

Fig. 9. Test network with inductive termination: comparison between measured (solid) and reference (dashed) values of the impedance matrix entries, in magnitude and angle.

minimal deviations between 80 MHz to 110 MHz. The overall accuracy is comparable with the analogous admittance formulation [36]. Furthermore, the dynamic range spans six order of magnitudes, and the complex frequency-dependent behavior of impedance angles is correctly identified in all configurations.

D. Effects of Different Probes on Measurement Accuracy and Frequency Range

In this section, the effect of different probes on the accuracy and frequency range of the proposed method is assessed by comparing the results obtained by the all three setups listed in Sec. IV.A. For brevity, a single test case (the inductive termination) is considered, and the relevant results obtained with setup III are already reported in Fig. 9. Results obtained with setup I and II are reported in Fig. 10 and Fig. 11, respectively.

The first comparison is made between setups III and I which are both very practical, as the cable under test is simply clamped

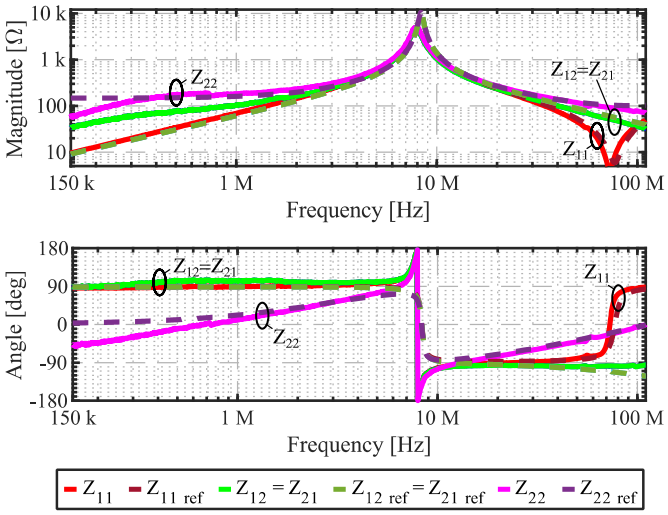

Fig. 10. Test network with inductive termination: comparison between impedance matrix entries reference values (dashed), in magnitude and angle, and measured values (solid) obtained by the setup with one FCC F-120-2 probe and one Solar 9123-1N with no external windings.

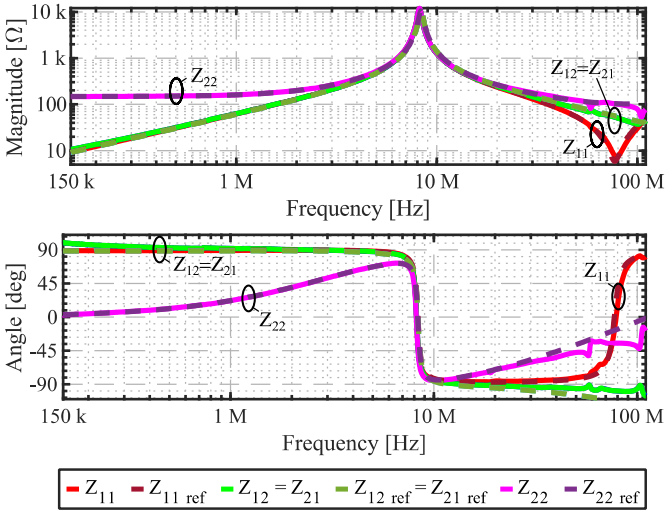

Fig. 11. Test network with inductive termination: comparison between impedance matrix entries reference values (dashed), in magnitude and angle, and measured values (solid) obtained by the setup with one FCC F-120-2 probe with a two-turn external winding and one Solar 9123-1N probe with a six-turn external winding.

(N_s=1). However, while setup III satisfies the suggested criterium N_s=N_p, setup I involves probes with many turns of the primary winding so N_s<N_p. By comparing Fig. 9 and Fig. 10, it is possible to observe that the setup I provides an overall comparable performance with setup III only between 10 MHz and 110 MHz. Conversely, setup I exhibits significant inaccuracy below 10 MHz, including magnitude errors in the very-low frequency range, and angle errors at the 8 MHz resonance. Hence, it is worth comparing again the accurate and practical setup III (Fig. 9) with setup II (Fig. 11). The latter uses the same probes of setup I but uses additional turns of the clamped cable to guarantee, for each probe, N_s=N_p. As a result, sensitivity is expected to improve at the expense of practicality. One can see that setup II solves the previous low-frequency issues of setup I, providing an overall good performance between 150 kHz and 30 MHz, definitely comparable to setup III. However, one can also notice that setup II exhibits relevant

angle errors at high frequency between 30 MHz and 110 MHz, especially on Z_{22}, unlike setup III. This happens because many hand-made cable turns introduce random and uncontrolled parasitic effects at high frequency, thus affecting accuracy and reproducibility. Overall, these experimental results fully support the criteria for probe selection identified in Section III.

V. Characterization of the In-Circuit Impedance Parameters of a Lead-Acid Battery

In this Section, an application example of the use of the proposed inductively coupled measurement method for EMI analysis is discussed. In particular, the impedance matrix $\mathbf{Z}_{Batt}$ of an automotive lead-acid battery is determined.

Generally speaking, an EUT impedance matrix $\mathbf{Z}_{EUT}$ can effectively be used as a representation of the passive part of a Thevenin circuit model, which, unitedly with suitable voltage sources V_{ThP} and V_{ThN}, describes the EUT as a multiport EMI source in the frequency domain [7], [8]. In this respect, the proposed inductively coupled in-circuit measurement method offers a straightforward solution to obtain the passive part of such a behavioral model. When considering batteries in particular, the characterization in terms of impedance matrix is sufficient, as batteries do not include any EMI source. Nevertheless, the proposed method is of great relevance for the characterization of modern high-power batteries, which can exhibit a dc voltage up to several hundreds of volts, thus preventing their characterization by VNAs or other RF instruments.

A. Experimental Setup

The considered experimental setup is shown in Fig. 12. The EUT is a lead-acid automotive battery, with earthed negative pole, which is fed by a Line Impedance Stabilization Network (LISN) through a cable with positive (P) and negative (N). The setup is arranged over a ground plane (G). The VNA (not shown) is set to span from 150 kHz to 110 MHz, with 100 Hz resolution bandwidth, and 8 dBm forward power.

Probes 1 and 2 are clamped on the P and N cables close to the battery terminals, as shown in Fig. 12 and schematized in Fig. 13(a). A reduced setup shown in Fig. 13(b) is used to separately measure the powerline (i.e., cable and LISN) impedance parameters. In this setup, the battery is disconnected, and its P and N wires are shorted to PE (while the LISN is clearly not fed by the power outlet).

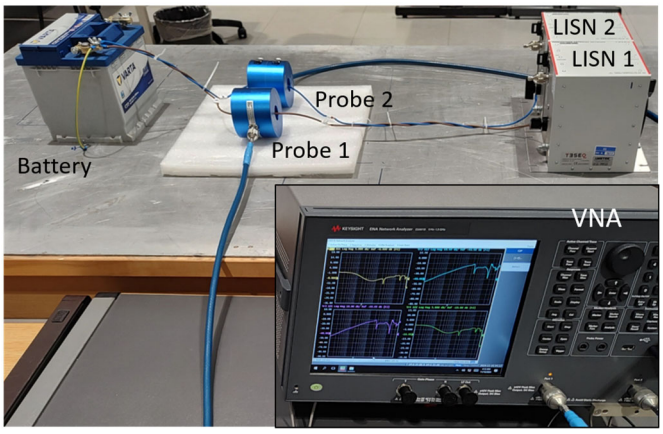

Fig. 12. Experimental setup for the measurement of the battery impedance matrix.

B. In-Circuit Impedance Measurement and De-embedding

The proposed measurement method is performed in the two setups shown in Fig. 13(a) and Fig. 13(c), resulting in two impedance matrices in the frequency range 150 kHz – 110 MHz. For the test setup reported in Fig. 13(a), the measured impedance matrix includes contributions from the whole circuital loop (battery, cable, LISN) and is therefore denoted as $\mathbf{Z}_{loop}$. For the second test setup, reported in Fig. 13(b), the impedance matrix includes contributions from the cable and LISN only, and is hereby called $\mathbf{Z}_{C\text{-}L}$.

To retrieve the battery impedance matrix $\mathbf{Z}_{Batt}$, the cable and LISN contributions are de-embedded from the whole loop. With reference to the variables depicted in Fig. 13(a), the following relationships hold:

$$\mathbf{v}_{Batt} = \mathbf{Z}_{Batt}\mathbf{i}_{Batt} \tag{16}$$

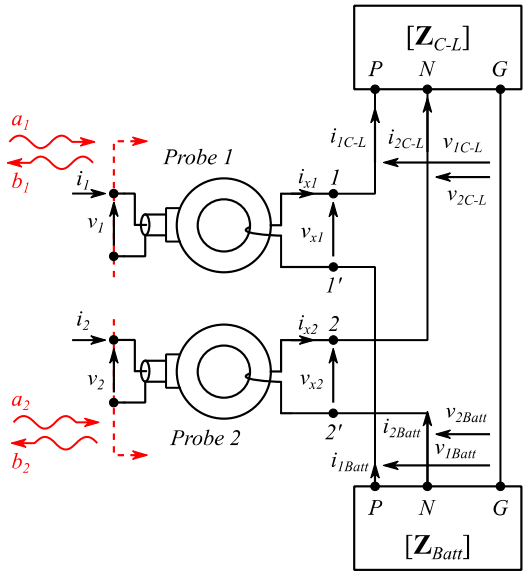

(a)

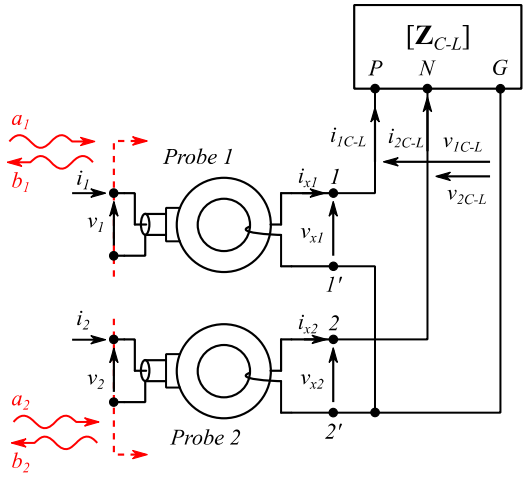

(b)

Fig. 13. Experimental setup for the measurement of the battery impedance matrix, (b) principle schematic, and (c) reduced setup for LISN and cable characterization.

$$\mathbf{v}_{C-L} = \mathbf{Z}_{C-L}\mathbf{i}_{C-L} \quad (17)$$

$$\mathbf{v}_{x} = \mathbf{Z}_{loop}\mathbf{i}_{x} \quad (18)$$

where $\mathbf{i}_{Batt} = [i_{1Batt}\ i_{2Batt}]^T$, $\mathbf{v}_{Batt} = [v_{1Batt}\ v_{2Batt}]^T$, $\mathbf{i}_{C\text{-}L} = [i_{1C\text{-}L}\ i_{2C\text{-}L}]^T$, $\mathbf{v}_{C\text{-}L} = [v_{1C\text{-}L}\ v_{2C\text{-}L}]^T$, $\mathbf{i} = [i_{x1}\ i_{x2}]^T$, $\mathbf{v} = [v_{x1}\ v_{x2}]^T$. Considering the circuit in Fig. 13(a), it is possible to appreciate that the following Kirchhoff laws hold:

$$\mathbf{i}_{x} = \mathbf{i}_{C-L} = -\mathbf{i}_{Batt} \quad (19)$$

$$\mathbf{v}_{x} = \mathbf{v}_{C-L} - \mathbf{v}_{Batt} \quad (20)$$

Combining (16)-(20) , it is easy to prove that the battery impedance matrix is obtained as

$$\mathbf{Z}_{Batt} = \mathbf{Z}_{loop} - \mathbf{Z}_{C-L} \quad (21)$$

C. Lead Acid Battery Impedance Parameters

By means of the method proposed in Section II and of the LISN and cables de-embedding procedure discussed in Section IV.B, the impedance matrix $\mathbf{Z}_{Batt}$ of the lead-acid battery depicted in Fig. 12 is obtained. A step-by-step overview of the overall procedure is presented in Table II. The magnitude and angle of the entries of the battery impedance matrix $\mathbf{Z}_{Batt}$ are reported in Fig. 14. The magnitude and angle of the entries of the battery modal impedance matrix, mathematically obtained by a modal transformation of voltages and currents [33], are reported in Fig. 15.

Considering the physical impedance in Fig. 14, one can note that, as expected [39], the self-impedances are mostly inductive and exhibit a smooth behavior, with the exception of the lowest frequency portion of the frequency response of the magnitude of Z_{22} which is affected by some measurement noise. This measurement noise is observed due to the magnitude of Z_{22} being more than one order of magnitude smaller than Z_{11} and close to the sensitivity limits of the proposed method in the considered setup (i.e. with the available probes).

Regarding the modal impedances in Fig. 15, it is worth observing that all impedances exhibit a smooth, inductive behavior up to around 20 MHz. The DM self-impedance is steadily quite larger than all other parameters, while the CM self-impedance is quite smaller, suggesting that the battery is a relatively low-impedance path for CM currents. Additionally, the mutual modal impedance is significant, and even larger than the CM self-impedance in most of the frequency range of interest, which may result in non-negligible mode conversion phenomena. This result strongly supports the relevance of the proposed method, as mutual modal impedances are otherwise impossible to measure in active, high-power devices, and ignoring their impact may result in severe inaccuracy in the prediction of conducted emissions.

TABLE II
OVERVIEW OF THE PROPOSED MEASUREMENT PROCEDURE

STEP 1	*Selection of suitable inductive probes according to the criteria discussed in Section III*
STEP 2	*Setup calibration: determination of the seven coefficients h_1, h_2, h_3, h_4, h_5, h_6, h_7 by the procedure discussed in Section II.B*
STEP 3	*S-parameters measurement of the setup in Fig. 12, in the presence - Fig. 13(a) - and in the absence – Fig. 13(b) - of the battery*
STEP 4	*Measurement post-processing: calculation of impedance matrices by eq. (6) - (9) and coefficients from Step 2*
STEP 5	*De-embedding of LISNs and cables contribution by eq. (21)*
STEP 6	*Optional - modal transformation of the obtained impedance matrix*

VI. CONCLUSION

In this work, an inductively coupled two-port in-circuit impedance measurement technique is discussed, which constitutes an extension of the traditional SPS for one-port impedance measurements and is obtained as an alternative formulation of the recently proposed MPS for two-port admittance measurement. The proposed method is suitable for the characterization of passive multiport systems as well as energized EUTs, and can accurately represents 2×2 impedance matrices, including mutual impedances, unlike previously available SPS techniques.

With respect to other comparable measurement techniques, the proposed impedance measurement method exhibits a number of advantages. First, the proposed method relies on VNAs, which cover the full frequency range of interest (up to 110 MHz), unlike impedance meters. Second, the VNA can be coupled to energized systems, as the probes provide sufficient attenuation of low-frequency voltages and currents related to

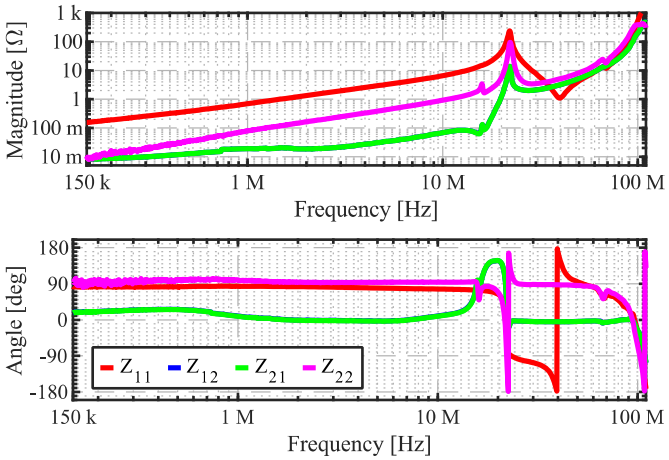

Fig. 14. Physical impedance matrix entries, in magnitude and angle, obtained from the characterization of the first battery sample.

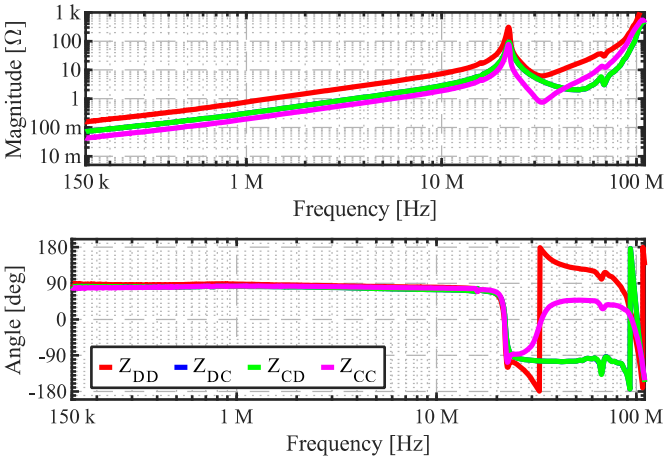

Fig. 15. Modal impedance matrix entries, in magnitude and angle, obtained from the characterization of the first battery sample.

the operation of high-power EUTs. The measurement procedure is hence not intrusive and does not require any alteration of the EUT, as the probes are simply clamped across its cables. Lastly, the proposed method allows the direct measurement of full impedance matrices, including mutual terms and with no need for numerical matrix inversions, which can then be mathematically converted into modal impedance matrices.

As the proposed method relies on inductive probes, its accuracy is strictly related to the TI and/or IL in the frequency range of interest, which makes correct probe selection crucial. To avoid issues related to the use of inefficient probes, the optimal probe selection criteria were discussed in detail. In particular, it has been shown that compensating the number of turns of the probe with an equal number of turns of the clamped cable is an appropriate action to optimize the accuracy of the measurement process. However, for large numbers of hand-made turns, the consequent lack of repeatability affects the accuracy at high frequencies.

The proposed measurement technique was experimentally validated by means of a set of tests performed on artificial passive networks, in the frequency range 150 kHz – 110 MHz, providing good accuracy over a wide range of impedance values, with magnitudes spanning over five orders of magnitude. As a practical implementation on a real-world system, the proposed method was applied to the characterization of an automotive battery, both in terms of physical and modal impedances. The results show significant coupling between CM and DM, supporting the need for a full matrix characterization. Perspective application include the characterization of power converters and other multiport power devices in real operating conditions, with the aim of developing behavioral models suitable for EMI simulation.

REFERENCES

[1] F. Fan, K. Y. See, X. Liu, K. Li and A. K. Gupta, "Systematic Common-Mode Filter Design for Inverter-Driven Motor System Based on In-Circuit Impedance Extraction," in *IEEE IEEE Trans. Electromagn. Compat.*, vol. 62, no. 5, pp. 1711-1722, Oct. 2020.

[2] V. Tarateeraseth, K. Y. See, F. G. Canavero, and R.W.-Y. Chang, "Systematic electromagnetic interference filter design based on information from in-circuit impedance measurements," *IEEE Trans. Electromagn. Compat.*, vol. 52, no. 3, pp. 588–598, Aug. 2010.

[3] S. Negri, G. Spadacini, F. Grassi and S. A. Pignari, "Black-Box Modeling of EMI Filters for Frequency and Time-Domain Simulations," in *IEEE Trans. Electromagn. Compat.*, vol. 64, no. 1, pp. 119-128, Feb. 2022.

[4] S. Negri, G. Spadacini, F. Grassi and S. A. Pignari, "Prediction of EMI Filter Attenuation in Power-Electronic Converters via Circuit Simulation," in *IEEE Trans. Electromagn. Compat.*, vol. 64, no. 4, pp. 1086-1096, Aug. 2022.

[5] L. Wan, S. Negri, G. Spadacini, F. Grassi, and S. A. Pignari, "Enhanced Impedance Measurement to Predict Electromagnetic Interference Attenuation Provided by EMI Filters in Systems with AC/DC Converters," *Applied Sciences*, vol. 12, no. 23, p. 12497, Dec. 2022.

[6] S. Negri, G. Spadacini, F. Grassi, P. Lezynski, R. Smolenski, and S. A. Pignari, "Comprehensive Comparison of Physical and Behavioral Approaches for Virtual Prototyping and Accurate Modeling of Three-Phase EMI Filters" in *Energies*, vol. 17, no. 19: 4974, 2024.

[7] A. C. Baisden, D. Boroyevich, and W. Fei, "Generalized terminal modeling of electromagnetic interference," *IEEE Trans. Ind. Appl.*, vol. 46, no. 5, pp. 2068–2079, Sep./Oct. 2010.

[8] H. Bishnoi, A. C. Baisden, P. Mattavelli and D. Boroyevich, "Analysis of EMI Terminal Modeling of Switched Power Converters," in *IEEE Trans. on Power Electron.,* vol. 27, no. 9, pp. 3924-3933, Sept. 2012.

[9] S. Kamala, N. B. Y. Gorla and S. K. Panda, "Small-Signal Stability Improvement of Microgrid With Battery Energy Storage System Based on Real-Time Grid Impedance Measurement," in *IEEE Transactions on Industry Applications*, vol. 58, no. 2, pp. 2537-2546, March-April 2022.

[10] S. B. Lee, R. M. Tallam, and T. G. Habetler, "A robust, on-line turnfault detection technique for induction machines based on monitoring the sequence component impedance matrix," *IEEE Trans. Power Electron.*, vol. 18, no. 3, pp. 865–872, May 2003.

[11] Z. Zhao, F. Fan, W. Wang, Y. Liu, and K. Y. See, "Detection of stator interturn short-circuit faults in inverter-fed induction motors by online common-mode impedance monitoring," *IEEE Trans. Instrum. Meas.*, vol. 70, 2021, Art. no. 3513110.

[12] D. -I. Stroe, V. Knap, M. Swierczynski and E. Schaltz, "Electrochemical Impedance Spectroscopy-Based Electric Circuit Modeling of Lithium–Sulfur Batteries During a Discharging State," in *IEEE Transactions on Industry Applications*, vol. 55, no. 1, pp. 631-637, Jan.-Feb. 2019.

[13] M. Tran, J. Sihvo and T. Roinila, "Internal Impedance in Determining Usability of Used Lithium-Ion Batteries in Second-Life Applications," in *IEEE Transactions on Industry Applications*, vol. 59, no. 5, pp. 6513-6521, Sept.-Oct. 2023.

[14] S. M. R. Islam and S. -Y. Park, "Precise Online Electrochemical Impedance Spectroscopy Strategies for Li-Ion Batteries," in *IEEE Transactions on Industry Applications*, vol. 56, no. 2, pp. 1661-1669, March-April 2020.

[15] A. A. Hussein and A. A. Fardoun, "An Adaptive Sensorless Measurement Technique for Internal Temperature of Li-Ion Batteries Using Impedance Phase Spectroscopy," in *IEEE Transactions on Industry Applications*, vol. 56, no. 3, pp. 3043-3051, May-June 2020.

[16] Y. Zhang *et al*., "Fault Diagnosis Method of Lithium-Ion Battery Leakage Based on Electrochemical Impedance Spectroscopy," in *IEEE Transactions on Industry Applications*, vol. 60, no. 1, pp. 1879-1889, Jan.-Feb. 2024.

[17] J. E. Timperley and J. M. Vallejo, "Condition Assessment of Electrical Apparatus With EMI Diagnostics," in *IEEE Transactions on Industry Applications*, vol. 53, no. 1, pp. 693-699, Jan.-Feb. 2017.

[18] Z. Zhao et al., "Voltage-dependent capacitance extraction of SiC power MOSFETs using inductively coupled in-circuit impedance measurement technique," *IEEE Trans. Electromagn. Compat.*, vol. 61, no. 4, pp. 1322–1328, Aug. 2019.

[19] K. R. Li, K. Y. See, and X. M. Li, "Inductive coupled in-circuit impedance monitoring of electrical system using two-port ABCD network approach," *IEEE Trans. Instrum. Meas.,* vol. 64, no. 9, pp. 2489–2495, Sep. 2015.

[20] A. Weerasinghe, Z. Zhao, N. B. Narampanawe, Z. Yang, T. Svimonishvili, and K. Y. See, "Single-probe inductively coupled in-circuit impedance measurement," *IEEE Trans. Electromagn. Compat.*, vol. 64, no. 1, pp. 2–10, Feb. 2022.

[21] R. A. Southwick and W. C. Dolle, "Line impedance measuring instrumentation utilizing current probe coupling," *IEEE Trans. Electromagn. Compat.*, vol. 13, no. 4, pp. 31–36, Nov. 1971.

[22] S. B. Rathnayaka, K. Y. See, and K. Li, "Online impedance monitoring of transformer based on inductive coupling approach," *IEEE Trans. Dielectrics Elect. Insul.*, vol. 24, no. 2, pp. 1273–1279, Apr. 2017.

[23] M. Prajapati, F. Fan, Z. Zhao, and K. Y. See, "Estimation of radiated emissions from PV system through black box approach," *IEEE Trans. Instrum. Meas.*, vol. 70, 2021, Art. no. 9004304.

[24] S. B. Rathnayaka *et al.*, "Inductively coupled on-line impedance measurement for condition monitoring of electrical equipment," *IET Sci., Meas. Tech.,* vol. 12, no. 3, pp. 382–387, May 2018.

[25] J. Rhee, H. Kim, K. Chu and S. Ahn, "Methodology for Extracting Low-Frequency Input Impedance of Personal Computer During Operation Using Dual Current Probes Method," in *IEEE Transactions on Electromagnetic Compatibility*, vol. 66, no. 2, pp. 584-598, April 2024.

[26] J. Ji, D. Zhang, T. Li and J. Lu, "Modeling of In-Circuit Impedance Measurement for SMPS Considering Power Noise Source," in *IEEE Transactions on Instrumentation and Measurement*, vol. 74, pp. 1-10, 2025, Art no. 9000310.

[27] Z. Zhao, A. Weerasinghe, W. Wang, E. K. Chua, and K. Y. See, "Eliminating the effect of probe-to-probe coupling in inductive coupling method for in-circuit impedance measurement," *IEEE Trans. Instrum. Meas.*, vol. 70, 2021, Art. no. 1000908.

[28] V.Tarateeraseth, B. Hu, K.Y. See, and F. G. Canavero, "Accurate extraction of noise source impedance of an SMPS under operating conditions," *IEEE Trans. Power Electron.,* vol. 25, no. 1, pp. 111–117, Jan. 2010.

[29] A. Weerasinghe, Z. Zhao, F. Fan, P. Tu and K. Y. See, "In-Circuit Differential-Mode Impedance Extraction at the AC Input of a Motor Drive System," *2021 Asia-Pacific International Symposium on Electromagnetic Compatibility (APEMC)*, Nusa Dua - Bali, Indonesia, 2021, pp. 1-4.

[30] Z. Zhao, F. Fan, A. Weerasinghe, P. Tu and K. Y. See, "Measurement of In-Circuit Common-Mode Impedance at the AC Input of a Motor Drive System," *2021 Asia-Pacific International Symposium on Electromagnetic Compatibility (APEMC)*, Nusa Dua - Bali, Indonesia, 2021, pp. 1-4.

[31] A. Weerasinghe *et al*., "A Novel Single-Probe Setup for Multifrequency Simultaneous Measurement of In-Circuit Impedance," in *IEEE Trans. Ind. Electron.*, vol. 70, no. 9, pp. 9538-9549, Sept. 2023.

[32] S. Negri, G. Spadacini, F. Grassi and S. A. Pignari, "Inductively Coupled In-Circuit Measurement of Two-Port Admittance Parameters," *IEEE Trans. Ind. Electron.*, accepted for publication, 2024.

[33] S. Negri, G. Spadacini, F. Grassi and S. A. Pignari, "Full Modal-Admittance Matrix In-Circuit Measurement by Multiple Inductive Probes," *2024 IEEE International Symposium on Electromagnetic Compatibility, Signal & Power Integrity (EMC+SIPI)*, Phoenix, AZ, USA, 2024, pp. 162-166.

[34] S. Negri, G. Spadacini, F. Grassi and S. Pignari, "Measurement-Based Equivalent Circuit Model for Time-Domain Simulation of EMI Filters," *2022 International Symposium on Electromagnetic Compatibility – EMC Europe*, Gothenburg, Sweden, 2022, pp. 793-798.

[35] S. Negri, G. Spadacini, F. Grassi and S. A. Pignari, "Non-Intrusive Measurement of Two-Port Impedance Parameters by Clamp-on Inductive Probes," *2024 IEEE International Conference on Environment and Electrical Engineering and 2024 IEEE Industrial and Commercial Power Systems Europe (EEEIC / I&CPS Europe)*, Rome, Italy, 2024, pp. 1-6.

[36] CISPR 25 Radio disturbance characteristics for the protection of receivers used on board vehicles boats and on devices-Limits and methods of measurement, IEC Geneva, 2002.

[37] M. Mardiguian, "Diagnostic, Troubleshooting Techniques, and Instrumentation", in *EMI Troubleshooting Techniques, 1st* ed. New York, USA: McGraw Hill Professional, 1999.

[38] S. Negri, G. Spadacini, F. Grassi and S. A. Pignari, "Accuracy Assessment of Non-Intrusive Measurement of Two-Port Impedance and Admittance Parameters by Inductive Couplers," *2024 IEEE International Symposium on Measurements & Networking (M&N)*, Rome, Italy, 2024, pp. 1-6.

[39] H. Hackl, D. J. Pommerenke, M. Ibel and B. Auinger, "Extraction of Single Cell Impedance From Battery Module Measurement by Simulation-Based De-Embedding," in *IEEE Transactions on Signal and Power Integrity*, vol. 1, pp. 112-120, 2022.

Simone Negri (M'20–SM'25) received the B.Sc. and M.Sc. (cum Laude) and PhD (cum Laude) degrees in Electrical Engineering from Politecnico di Milano, Milan, Italy, in 2014, 2016, and 2020, respectively.

He is currently an Assistant Professor with Department of the Electronics, Information and Bioengineering (DEIB), Politecnico di Milano, where he has been a Postdoctoral Research Fellow from 2019 to 2022. His research interests are mostly in the field of Electromagnetic Compatibility (EMC), and include EMI filters and electronic power converters modelling and conducted emissions evaluation and prediction. Further research interests include power converters modelling and control, application of advanced control and optimization techniques in power systems, hybrid AC/DC distribution systems, and power quality and reliability.

Dr. Negri is the recipient of the 2023 International Union of Radio Science (URSI) "Roberto Sorrentino" Young Scientist Best Paper Award, and he is active in the standardization of LVDC systems as a Member of the CEI (Italian Electrotechnical Committee) CT 320 technical committee, where he is the convenor of the working group GdL1, Member of several IEC SyC LVDC working groups, and Member of the European Commission SET Plan TWG - LVDC.

Giordano Spadacini (M'07–SM'16) received the Laurea (M.Sc.) and Ph.D. degrees in electrical engineering in 2001 and 2005, respectively, from Politecnico di Milano, Italy, where he is currently an Associate Professor with the Dept. of Electronics, Information and Bioengineering. His research interests include statistical models for the characterization of interference effects, distributed parameter circuit modeling, experimental procedures and setups for EMC testing, and EMC in aerospace, automotive and railway systems.

Dr. Spadacini is a recipient of the 2005 EMC Transactions Prize Paper Award, the 2016 and the 2021 R. B. Schulz Best EMC Transactions Paper Award, two Best Symposium Paper Awards from the 2015 Asia-Pacific Int. Symp. on EMC (APEMC) and the 2018 Joint IEEE EMC & APEMC Symposium.

Flavia Grassi (M'07–SM'13) received the Laurea (M.Sc.) and Ph.D. degrees in electrical engineering from Politecnico di Milano, Milan, Italy, in 2002 and 2006, respectively.

She is currently a Full Professor in the Department of Electronics, Information and Bioengineering, Politecnico di Milano. From 2008 to 2009, she was with the European Space Agency (ESA), ESA/ESTEC, The Netherlands, as a Research Fellow. Her research interests include distributed-parameter circuit modeling, statistical techniques, characterization of measurement setups for EMC testing (aerospace and automotive sectors), and application of the powerline communications technology in ac and dc lines.

Dr. Grassi received the International Union of Radio Science (URSI) Young Scientist Award in 2008, and the IEEE Young Scientist Award at the 2016 Asia- Pacific International Symposium on EMC (APEMC), the IEEE EMC Society Transactions Prize Paper Award in 2016 and 2021, and the Best Symposium Paper Award at the 2015 and 2018 APEMC. She is currently serving as an Associate Editor of the IEEE Transactions on Electromagnetic Compatibility, IEEE EMC

Magazine, and IEEE Letters on Electromagnetic Compatibility Practice and Applications.

Sergio A. Pignari (M'01–SM'07–F'12) received the Laurea (M.S.) and Ph.D. degrees in electronic engineering from Politecnico di Torino, Turin, Italy, in 1988 and 1993, respectively.

From 1991 to 1998, he was an Assistant Professor with the Dept. of Electronics, Politecnico di Torino, Turin, Italy. In 1998, he joined Politecnico di Milano, Milan, Italy, where he is currently a Full Professor of Circuit Theory and Electromagnetic Compatibility (EMC) at the Dept. of Electronics, Information, and Bioengineering, and Chair of the B.Sc. and M.Sc. Study Programmes in Electrical Engineering, term 2015-20. He is the author or coauthor of more than 200 papers published in international journals and conference proceedings. His research interests are in the field of EMC and include field-to-wire coupling and crosstalk, conducted immunity and emissions in multi-wire structures, statistical techniques for EMC prediction, and experimental procedures and setups for EMC testing. His research activity is mainly related to Aerospace, Automotive, Energy, and Railway industry sectors.

Dr. Pignari is co-recipient of the 2005, 2016, and 2021 IEEE EMC Society Transactions Prize Paper Award, and a 2011 IEEE EMC Society Technical Achievement Award. He is currently serving as an Editor-in-Chief of the IEEE Transactions on Electromagnetic Compatibility. From 2010 to 2015 he served as the IEEE EMC Society Chapter Coordinator. From 2007 to 2009 he was the Chair of the IEEE Italy Section EMC Society Chapter. He served as the Italian URSI Officer for Commission E (Electromagnetic Noise and Interference), term 2015-18. He served as Technical Program Co-Chair of the ESA Workshop on Aerospace EMC in 2009, 2012, 2016 and 2019, and as Member of the Technical Program Committee of the Asia Pacific EMC Week since 2010.